Accepted Manuscript

Blast response of aluminium/thermoplastic polyurethane sandwich panels – experimental work and numerical analysis

A. Jamil , Z.W. Guan , W.J. Cantwell , X.F. Zhang , G.S. Langdon , Q.Y. Wang

PII: S0734-743X(17)30643-7
DOI: https://doi.org/10.1016/j.ijimpeng.2019.01.003
Reference: IE 3226

To appear in: *International Journal of Impact Engineering*

Received date: 28 July 2017
Revised date: 30 December 2018
Accepted date: 7 January 2019

Please cite this article as: A. Jamil , Z.W. Guan , W.J. Cantwell , X.F. Zhang , G.S. Langdon , Q.Y. Wang , Blast response of aluminium/thermoplastic polyurethane sandwich panels – experimental work and numerical analysis, *International Journal of Impact Engineering* (2019), doi: https://doi.org/10.1016/j.ijimpeng.2019.01.003

Highlights

- Novel sandwich structure subject to blast loading using PE4 explosives
- Experimental and numerical work is covered
- Thermoplastic polyurethane (TPU) is shown to be a promising material under blast
- Pave the way for future design and development using this material

Blast response of aluminium/thermoplastic polyurethane sandwich panels – experimental work and numerical analysis

A. Jamil[a], Z.W. Guan[a,b,*], W.J. Cantwell[c], X.F. Zhang[d], G.S. Langdon[e], Q.Y. Wang[b]

[a]*School of Engineering, University of Liverpool, Liverpool L69 3GH, UK*
[b]*School of Mechanical Engineering, Chengdu University, Shiling Town, Chengdu City, Sichuan Province, PR China*
[c]*Department of Aerospace Engineering, Khalifa University of Science and Technology (KUST), Abu Dhabi, United Arab Emirates*
[d]*School of Mechanical Engineering, Nanjing University of Science and Technology, Nanjing 210094, Jiangsu Province, PR China*
[e]*Blast and Impact Survivability Research Unit (BISRU), Department of Mechanical Engineering, University of Cape Town, Rondebosch 7700, South Africa*

Abstract

This article presents experimental and numerical results following blast tests on a polyether grade thermoplastic polyurethane (TPU). Aluminium alloy (AA) 2024-T3 skins were used as facings to enhance the blast resistance of sandwich structures with TPU cores and varying thicknesses. The experimental results highlighted an improvement in blast resistance with the addition of skins to the TPU core. Increasing the thickness of the TPU core in the sandwich panels served to increase the blast resistance of the structure. For example a 20 mm core offered a blast resistance that was 50.2 % higher than an equivalent 5 mm core and 71.2 % higher than a plain (i.e. no skin) 5 mm TPU core. Numerical simulations of the blast response of the TPU panels were conducted by converting the explosive loading regime applied to the panels to a simplified pressure pulse loading. Good agreement was obtained between the numerical and experimental results for the back face deflection profiles through the central cross-sections of the panels.

Keywords:
blast mitigation, finite element, sandwich panel, SHPB, structural response, thermoplastic polyurethane

* Corresponding author
Email address: zguan@liverpool.ac.uk

1. Introduction

History presents evidence of the risk and repercussions of explosions to both structural integrity and consequently human life. Due to this, a great deal of effort has been expended by the engineering community as well as government agencies to improve the impact and shock resistance of engineering structures. Several studies have been carried out on the development of sandwich structures that are able to withstand high-intensity impulse loading [1–7]. Sandwich constructions that can be traced back to the middle of the 19th century [8] are known to be efficient energy absorption systems and have since been exploited for their weight to stiffness ratios, high structural efficiency and durability. These structures have important applications in both the aerospace and naval industry, fundamentally due to their properties, i.e. dissipating the impulse that is transmitted to the structure.

Polymers are increasingly used as core materials in sandwich structures [5, 9–11], and are popular due to their low cost, ease of production, corrosion resistance and relatively low density. With very high ductility and good stress-strain recovery under both compression and tension, thermo- plastic polyurethane (TPU) is considered as one of the most versatile plastic materials compared to regular rigid plastics [12]. A study carried out by Jamil *et al.* [13] investigated TPU under impact loading, where the specific energy absorption characteristics showed a proportional increase with increased impact energy. The TPU also had the ability to recover from such severe loading conditions, a phenomenon which is not apparent for metal based cellular solids such as honeycombs.

A blast wave describes the layer of compressed air that lies in front of the hot gas that is generated due to detonation of an explosive, which contains most of the energy released by the explosion. The blast wave pressure time history is characterised by both positive and negative specific impulses and by its peak value of over-pressure above the ambient value. Figure 1 shows a typical pressure-time history for a blast wave. This over pressure decays as the blast wave expands away from the source of the explosion [14]. The simulation of such blast events is frequently complex and requires consideration of the blast wave pressure-time history as well as special consideration of the structural response to the blast loading event [15]. Blast loads usually involve very high strain-rates in the range of $10^3 - 10^4\ s^{-1}$; such high strain-rates (loading rates) could change the dynamic and mechanical properties of the target structures and consequently modify the expected damage mechanisms for various structural elements.

Analysing the effects of blast loading on structures requires a balance between computational cost and accuracy. Many studies employ simplistic blast loading conditions and structural models. However, challenges arise when modelling complex structures with complex geometries [16]. Nevertheless, a simplistic blast

loading approach has proven to be reliable for many types of structures subjected to uniform blast loading. The impulsive loading theory enables the simplification of the pressure-time history, as long as the impulse is represented accurately. Farrow *et al.* [17] investigated the use of both rectangular and triangular pressure pulse loading for the prediction of mid-point deflections, deformation shapes, residual strains and dynamic yield stress of circular plates subjected to uniform blast loading, using the ABAQUS finite element software package [18].

The aim of this study was to investigate TPU under high-intensity impulse loading, i.e. air blast. Here, the structural response of TPU panels, subjected to uniform blast loading, was investigated using a ballistic pendulum. The work was then extended to investigate the response of sandwich panels with aluminium alloy (2024-T3) skins and the TPU as the core material. Impulsive loads were increased to yield Mode I (large inelastic deformation), Mode II* (partial tearing along the boundary) and Mode II (tensile tearing around the full boundary) failure modes [19]. This is an investigation to evaluate the potential of such applications for blast mitigation, for potential use in applications such as luggage containers for aircraft or military vehicles. The TPU was characterised through a series of quasi-static and split-Hopkinson pressure bar (SHPB) and blast tests. The mid-point displacements and deformation modes of the panels were modelled using an ABAQUS/Explicit solver [18].

2. Sample preparation and experimental procedure

2.1. Specimen manufacture

The polyether grade TPU pellets (Desmopan DP 9852 [20]) were pre- dried at 110 °C for 3 hours. Plates were then manufactured using a hot press with a pressure of 350 kPa and a temperature of 220 °C (melting point) for 25 minutes. The TPU panels were then cooled at room temperature and removed from the 150 x 150 mm^2 moulds when the temperature was below 50 °C. The samples were then washed in distilled water, followed by washing in ethanol in order to remove any contamination. Further information on the manufacturing process of the TPU panels is available in an earlier paper [13]. Aluminium alloy (AA) 2024-T3 skins (1.2 mm thickness) were bonded to the TPU core using a fast-curing contact adhesive (Timebond) to fabricate sandwich panels with three core thicknesses of, 5, 10 and 20 mm.

2.2. Experimental procedure

2.2.1. Quasi-static testing

Quasi-static material tests were carried out in order to characterise the properties of the TPU polymer. Tensile tests were conducted on TPU specimens in accordance with ASTM D638 (type V dog-bone shaped specimens with a gauge length - 9.5 mm, width - 3.2 mm, thickness - 3 mm). Tests at low strain-rates were

carried out on an INSTRON 3369 universal test ma- chine, at cross-head displacement rates of 1, 10 and 100 mm/min. Standard laboratory conditions were 23±2 ˚C with 30-40 % relative humidity. The TPU was tested at three different orientations (0˚, 45˚ and 90˚), which were manufactured from a single TPU panel as shown in Figure 2, in order to determine whether there is any possible material anisotropy [11]. Tests were also undertaken on the aluminium alloy (AA 2024-T3), where tensile specimens with a thickness of 1.2 mm, were prepared and tested in accordance with ASTM E8/E8M (subsize specimen).

An extensometer was used to measure the initial extension of the TPU samples. The experimental method used for the tensile experiments does not take into account local measurements of true stress, true strain and true strain-rate after the onset of necking. Therefore, nominal stress, strain and strain-rate were used to characterise the overall response of the TPU and AA 2024-T3 specimens under tension.

2.2.2. Split-Hopkinson Pressure Bar (SHPB)

High strain-rate compression testing was performed on a split-Hopkinson pressure bar (SHPB) apparatus at Nanjing University of Science and Technology, PR China. Figure 3 shows a schematic illustration of the SHPB test set-up. Solid aluminium (7A04 T6) pressure incident and transmission bars were used, both of which have a length of 1 m and a diameter of 14.5 mm. The cylindrical specimens used for these tests had a thickness-to-diameter ratio of 1:1, with 8, 6 and 4 mm thicknesses being used in accordance with the strain-rate requirements. A shorter specimen length was necessary in order to generate a uniaxial stress state during pulse transmission. Furthermore, in order to obtain a homogenous deformation state, a thin layer of petroleum jelly was applied on both sides of the specimen and the end faces of the incident bar and the transmission bar to lubricate the contact surfaces. A pulse-shaping technique was also employed to ensure a constant strain-rate, smoothing the stress pulse, eliminating the high frequency oscillations in the incident pulse and extending the pulse duration in order to achieve stress equilibrium [21]. The chosen pulse-shaper material for this test was rubber and attached to one end of incident bar by a thin layer of grease with a thickness of 3 mm and thickness-to-diameter ratio ranging from 0.38 to 0.65. A digital oscilloscope with a 50 x 10^6 s^{-1} sampling rate capacity was used, to collect the test data. The filter method used in oscilloscope is the Arithmetic Mean Method, with 50 KHz lowpass filtering. The filter method adopted in Matlab is fir1 lowpass filtering and FFT filtering (Fast Fourier Transform Algorithm). The fir1 filtering function is b=fir1 (N, w_n), in which

N is the filter order, w_n is the cutoff frequency and b is the nth-order lowpass filter coefficient vector. The function fftfilter is y = fftfilter（b, X）, in which X is a data vector. Here, we choose w_n =0.01, N =50 in the function based on the experience.

In order to ensure the stress equilibrium, we sum the absolute data of the transmit wave and the reflect wave, and synchronise them with the values obtained for the absolute incident wave. The consistency of the two curves confirms the stress equilibrium, which is shown in Figure 4.

For each strain-rate, three repeated tests were carried out, with the standard deviation no more than 20%. The data for each test were smoothed twice, with the first one in the oscilloscope and the second one in the data processing.

2.2.3. Blast testing

The blast tests were carried out on a ballistic pendulum at the University of Cape Town, South Africa. In preparation for testing, four 12 mm diameter holes were drilled into the specimens to facilitate their positioning on the rig. The samples were bolted to the test set-up to provide a clamped boundary condition. The 150 x 150 mm panels were clamped between two steel frames, giving an exposed circular area with a diameter of 90 mm. Blast loading was applied by detonating a circular PE4 disk at a 90 mm stand- off distance (SOD). The PE4 plastic explosive was shaped into a cylindrical geometry, as described by Nurick *et al.* [22] and was placed onto a 14 mm thick polystyrene foam pad that was centrally located on the circular exposed area. The electrical detonator was then attached to the centre of the PE4 disk using one gram of additional explosive, known as a "leader". In order to direct the blast wave towards the sample, an open-ended transmission tube was bolted to the front clamping frame and the explosive was positioned at the open end, as shown in Figure 5.

The impulse generated by the blast loading was calculated using the natural period of the ballistic pendulum and results captured from the loading scenario. Figure 6 is a schematic representation of the ballistic pendulum and the associated geometry of the system. A laser displacement sensor (LDS) with a 100 x 10^6 s^{-1} sampling rate was connected to an oscilloscope, in order to calculate the displacements (X_1 and X_2) from the oscillations generated from the blast loading. The dashed lines indicate the position of the pendulum in maximum forward (blue) and backward (red) positions due to a blast load. This generates a sine wave output for the oscilloscope reading, a typical example of which is shown in Figure 7. The natural period of the pendulum was found by manually displacing the pendulum and releasing it in order to capture the time taken for a number of oscillations (typically 15), which was then averaged in order to establish the time taken for one oscillation.

Uniformity of the blast load on the target plate was assumed by employing a SOD greater than or equal to the radius of the plate [23]. In the case of a circular target, if the SOD is less than the radius of the target plate, the plate is assumed to be subjected to localised loading. If the SOD is larger than the radius of the target panels, then the blast load can be assumed to act uniformly [23].

3. Experimental results and discussion

3.1. Quasi-static testing

One of the disadvantages of considering anisotropic material models is the number of parameters that need to be identified; usually up to ten different types of experimental tests are required to measure the key mechanical properties [24]. For simplicity, many engineers and designers prefer to use isotropic material models in order to predict the mechanical behaviour of anisotropic materials, in order to save time and cost for experimental testing [24]. Nevertheless, in many TPUs, the hard domains are immersed in a soft (rubbery) matrix [25]. Since hard domains occupy a significant volume and are stiffer than soft domains, they function as an effective nanoscale filler [12]. Therefore, it was necessary to determine whether the current TPU exhibited any form of anisotropic behaviour. Figure 8 indicates that the TPU exhibits very little material anisotropy, with there being minor changes in the material behaviour at 0°, 45° and 90° directions. Based on this analysis, it is reasonable to assume the material is isotropic [11]. The effect of strain-rate on failure strain is shown in Figures 9a and 9b, where it is evident that the strain at failure increases with increasing strain-rate, highlighting a distinct strain-rate sensitivity in the TPU.

3.2. Characterisation of TPU at high strain-rates

The strain-rate sensitivity of the TPU was evaluated using Hopkinson bar compression rig, where a typical data acquisition was conducted by recording the voltage signals measured in the incident bar and transmitted bar of the Hopkinson bar apparatus. The strain-rate in the test sample, which was determined by the velocity of the input bar, was varied by adjusting the pressure in the main chamber of the gas gun.

Figure 10 shows plots of true stress versus true strain curves of different strain-rates, with the behaviour showing a strong rate dependence. The true stress-strain relationships highlight appreciable strain-rate effects in the response of the TPU polymer over six decades of strain-rate. The stress levels increase continuously with increasing strain-rate. There was no visible evidence of failure at strain-rates below 5000 s^{-1}. However, at a strain-rate of 7170 s^{-1}, fracture initiated on the impact face and macrocracks were visible at 8316 s^{-1}. Overall, the shape tendency of the stress-strain curves remains similar at higher strain-rates, with an apparent strain

hardening period after initial loading. Furthermore, it is evident that the stored strain energy re- lease of the TPU increases with increasing strain-rate, which could be useful under shock loading conditions. This phenomenon of increased energy release is related to the ability of the TPU to alter its microstructure and thus its mechanical behaviour [13]. Access to such strain rates enables precise characterisation of the strong dependence of the stress-strain behaviour for increased strain-rate loading.

3.3. Blast results and discussion

A limited number of tests were carried out on TPU samples with and without skins. Table 1 provides a description of the specimens tested under blast, and Table 2 shows the response of these specimens, including impulse (Ns), and the residual mid-point deflection of the back face. The diameter of the explosives was increased from 20 mm to 30 mm due to the limitations for the charge height to diameter ratio [22]. That is, for a certain diameter, increasing the explosive mass results in an increase in height, which influences the impulse generated by the explosive. Therefore, the diameter of the explosive has to be adjusted to increase the impulse. The impulses generated by the 20 mm diameter explosives were in the range of 11.8 - 15.8 Ns and those for the 30 mm explosives in the range of 14.1 - 24.6 Ns. Table 2 details the various failures observed in each of the samples, i.e. Mode I (large inelastic deformation), Mode II* (partial tearing around the boundary) and Mode II (tensile tearing around the full boundary).

For the TPU specimens without skins, an increased deflection was observed with increasing mass of explosive, until partial tearing was observed following testing with 12 grams of PE4. Figure 11 shows the failed A5 sample following blast without AA 2024-T3 skins, whereas Figure 12 shows the failure of the back face of a TPU sandwich panel (C3). Both panels exhibit a partial tearing (mode II*) failure mode. It should be noted that post-mortem removal of the skins, revealed that the TPU underwent a high degree of recovery i.e. no permanent deformation. The stress-wave propagation through the multi-layered material and the rebound of the TPU core caused the adhesive to fail, whilst the AA 2024-T3 skins continued to experience plastic deformations without rebound.

The low failure strain of a material is one of the limiting factors in the performance of composite laminates such as fibre reinforced plastics (FRPs) [26]. An example of which can be seen in the work undertaken by Yahya *et al.* [27], where it can be seen that the TPU outperforms most of the T300 carbon fibre-reinforced poly-ether-imide (CF/PEI) panels. One of the CF/PEI panels tested by Yahya *et al.* [27] had an average thickness of 8.22 mm and a density of 1510 kg/m^3, providing a much higher mass per unit area than that of the TPU panels (without skins), which has a density of 1150 kg/m^3. Yet complete failure, i.e.

matrix cracking, delamination, fibre buckling and fibre fracture, was observed following the test with just 8 grams of PE4. This is particularly critical in blast loading, due to the high strain- rate impulsive loadings that are involved. Therefore, the search in finding a material which possesses a higher strain to failure property would be expected to perform better in blast and impact loadings [26].

The plain TPU (i.e. without skins), with a 5 mm thickness, was able to withstand up to 11 grams of PE4 explosive, with failure occurring at 12 grams, illustrating the versatility and toughness of TPU. Further tests were carried out on sandwich panels with cores having various thicknesses. Increases in the impulse resistance were seen with the addition of AA 2024- T3 skins, relative to the plain TPU, however, further increases were observed in relation to core thickness, where increases of 14.0, 23.8 and 71.2 % are observed for core thicknesses of 5, 10 and 20 mm, respectively. Table 3 provides a brief comparison of various panels tested in previous studies on the ballistic pendulum, indicating average areal density (kg/m^2), approximate material cost (GBP/kg) and resistance to impulse (Ns) prior to failure. In comparison, TPU alone (without AA 2024-T3 skins) is a relatively low cost and lightweight alternative with promising results for blast mitigation.

4. Plasticity modelling

For the numerical study, the TPU was modelled as an isotropic elasto- plastic material that exhibits strain rate-dependency utilising the Cowper- Symonds power law [28]. The total strain-rate can be decomposed into an elastic component, $\dot{\varepsilon}^{el}$, and a plastic component, $\dot{\varepsilon}^{pl}$. Generally, the plastic flow stress, σ_{pl}, of a material can be expressed as,

$$\sigma_{pl} = f(\varepsilon_{pl}) \cdot R(\dot{\varepsilon}) \tag{1}$$

where f is the quasi-static stress-strain behaviour imported into ABAQUS from the true stress-strain curves, R represents the ratio of the yield stress at any strain-rate to the static yield stress and $\dot{\varepsilon}$ represents the strain-rate.

In order to incorporate strain-rates effects in the TPU, the Cowper- Symonds model is used as follows,

$$\dot{\varepsilon}_{pl} = D(R-1)^p \tag{2}$$

The following power-law relationship is given as,

$$\sigma_s = \sigma_0 \left[1 + \left(\frac{\dot{\varepsilon}_{pl}}{D} \right) \right]^{1/p} \tag{3}$$

Here, $\dot{\varepsilon}^{pl}$ is the strain-rate and, σ_s and σ_0 represent the yield stress at the higher strain-rate and the static yield stress, respectively. *D* and *p* are material parameters, which can be determined from the SHPB tests by a regression procedure [29]. The coefficients for the Cowper Symonds parameters, D and p, were subsequently determined from the SHPB tests to be 971 s^{-1} and 0.98, respectively. The material properties for the TPU are given in Table 4, and the isotropic hardening data for the TPU polymer are provided in Table 5. Ductile failure criterion available in ABAQUS/Explicit [18] was used to simulate failure of the TPU.

The mechanical response of the TPU under in-plane compressive and tensile loading was predicted prior to the blast simulations. Figure 13 compares the experimental and numerical load-displacement, for the TPU under compressive and tensile loading conditions with negligible difference in the yield and plastic flow characteristics, highlighting a very good agreement between the predicted and measured responses.

The 2024-T3 aluminium alloy used for the skins, was modelled using the Johnson-Cook constitutive model [30] with rate-dependent hardening as follows,

$$\bar{\sigma} = [A + B(\bar{\varepsilon}_{pl})^n \left[1 + C \ln \left(\frac{\dot{\bar{\varepsilon}}_{pl}}{\dot{\varepsilon}_0} \right) \right] \tag{4}$$

where $\bar{\sigma}$ is equivalent stress, $\bar{\varepsilon}_{pl}$ is the equivalent plastic strain, *n* is a strain hardening index, $\dot{\bar{\varepsilon}}_{pl}$ is the equivalent plastic strain-rate and $\dot{\varepsilon}_0$ is the reference strain-rate. A, B, C and M are material constants. These material parameters [31], together with elastic properties used to model the aluminium alloy, are provided in Table 6. The parameters A and B have been determined from the earlier tensile stress-strain relationship obtained in this study.

The Johnson-Cook damage law [30] is widely used to provide a simple mathematical relation which describes the effects of stress triaxiality, strain-rate and temperature on the equivalent strain to ductile fracture. The failure strain of the alloy was modelled as,

$$\varepsilon_f = \left[D_1 + D_2 \exp \left(D_3 \frac{P}{\bar{\sigma}} \right) \right] \left[1 + D_4 \ln \left(\frac{\dot{\bar{\varepsilon}}}{\dot{\varepsilon}_0} \right) \right] \tag{5}$$

where ε_f is the equivalent strain to fracture at the current conditions of strain-rate, pressure and equivalent stress, P is a pressure stress, $D1 - D4$ (0.130, 0.130, -1.500, 0.011) are four non-dimensional material constants.

5. Blast modelling

The high temperatures generated by the fireball in an explosive event are extremely short in duration relative to the response of a sandwich panel. For materials which are thermal insulators (such as polymers), the thermal inertia of the core will be high and thus the high temperature duration of the fireball will not be transferred to the sandwich core. The skins of the sandwich are present to protect the core from catching fire in any case.

The modelling of structures under blast loading usually neglect the heating effects from the fireball for these reasons and consider only the shock pressure loading arising from the blast. Secondary fires (not from the primary blast event and fireball) are not considered in this work. During the post-test inspection of the sandwich panels, there were no signs of heating damage (either discolouration of the TPU or signs of melting and reforming) in the cores, or on the blasted surface of the skins.

The actual pressure-time loading associated with an explosion is a complex decaying pressure oscillation that may require simplification when modelling the effects of blast on structures. In order for one to use rectangular pressure pulse loading for a complex pressure distribution over the blast area, impulsive loading theory can be implemented, so long as the impulse is represented accurately. Due to inertia, the blast impulse can be transferred to the plate before the plate starts deforming. The pressure loading with the implementation of a rectangular [17, 32] or triangular [17] pulse, applied to the exposed blast area for a certain time. The time in this instance is identified once the intensity of the pressure pulse provided a negligible contribution to the deformation of the panels. The pressure pulse can be defined as,

$$P_{SO} = \frac{I_m}{A_T} \tag{6}$$

where, P_{SO} is the peak overpressure, I_m the measured impulse from the experiment, A the blast area on the plate tested and τ is the blast load duration.

The computational cost can be reduced by using the inherent symmetry of the problem. Therefore, only one quarter of the panel was modelled with appropriate boundary conditions applied along the planes of symmetry. The mesh, dimensions, loading (uniform) and boundary conditions are shown in Figure 14, for the panels

with and without AA 2024-T3 skins. In all cases eight-noded, linear hexahedral C3D8R elements with reduced integration and hourglass control were used. Mesh sensitivity studies were carried out to determine a 1 mm global element size, which demonstrated sufficient accuracy of the numerical results and mesh convergence rate. Surface to surface con- tact conditions between the core and facesheets were introduced. For the pressure pulse loading on the model, a triangular pulse was applied, as rep- resented by Equation 7. The pressure in this case was assumed to increase linearly up to the peak and return back to zero. The blast load duration for the simulations were taken as 360 μs.

$$P(t) = \begin{cases} \frac{2P_{SO}}{\tau} \cdot t, \ 0 < t < \tau/2 \\ 2P_{SO} - \frac{2P_{SO}}{\tau} \cdot t, \ \tau/2 < t < \tau \end{cases} \quad (7)$$

6. Blast simulation results and discussion

The typical displacement vs. time history together with the typical de- formation and debonding process of the blast simulations can be seen in Figure 15. Here, sufficient time was allowed within the simulation to allow any oscillations of the Lagrangian model to subside sufficiently.

The numerically predicted cross-section responses of the various panels following blast loading conditions, as shown in Figures 16 and 17, prove to be reasonably accurate. The deformation profiles indicate a very good correlation for the core of the TPU without skins as well as the TPU with AA 2024-T3 skins. The separation of the TPU core and AA 2024-T3 skins (Figure 17) are consistent in all cases, where some rebound of the TPU was observed for the simulations, as was the case with the experiments. A more quantitative representation of the mid-point displacement is also presented, where small differences (<10%) are observed for the mid-point displacements between the experimental and numerical responses of the panels. In order to provide a more direct comparison of deformation profiles, typical measured and the predicted displacements through the central cross section are provided (A1, A4, B1 and B3), which are shown in Figure 18. Here, due to the symmetric nature, only half of the profile is displayed, i.e. from the fixed boundary to the centre of the panel (0 – 45 mm). In general, the predicted displacements match with the experimental ones reasonably well. It is worth pointing out that for TPU panels without aluminium skins the predicted displacement profile is proportionally higher than that of the tested one (Figure 18a). This is due to the large deformation recovery of the TPU which is not simulated fully. However, the panels with aluminium skins show a less recovery

after blast due to the restraint offered by aluminium, so that there are small discrepancies in the chart (Figure 18b).

Figure 19 shows the numerical response of specimen C3 (Figure 12). Here the impulse applied was increased in accordance with the experimentally recorded impulse to establish partial tearing failure of the back face. It should be noted that in order to achieve this failure mode, a full model was necessary to allow for the asymmetric response of the back face.

7. Conclusions

The results of an investigation on the response of thermoplastic polyurethane (TPU) sandwich panels subjected to blast loading has been reported. TPU exhibited a strain-rate sensitivity under high strain-rate loading, as established by a series of split-Hopkinson pressure bar (SHPB) tests, indicating significant strain energy potential under high strain-rate loading. The TPU under blast loading was also shown to withstand relatively high PE4 explosive masses (up to 11 grams), providing a lightweight and low cost alternative to various other materials. The addition of aluminium alloy 2024-T3 skins as a basis of a sandwich construction provided additional resistance to impulsive loads. Increases in the blast resistance relative to the plain 5 mm TPU of 14.0, 23.8 and 71.2 % were observed with the addition of AA 2024-T3 skins and increases in the core thicknesses of 5, 10 and 20 mm, respectively. A further study was carried out to simulate uniform blast loading on the TPU panels, where a Cowper-Symonds strain-rate hardening model was adopted for the TPU based on SHPB test data. Using a simplified pressure pulse loading, both the simulated qualitative and quantitative responses were shown to have very good correlation to the experimental data, with negligible differences in the mid-point deflections and the back face deformation profiles through the central cross-sections of the panels. In order to achieve partial tearing failure of the back face of a panel, the numerical impulse was increased relative to the experimentally recorded impulse to match the failure experienced in the experimental study.

Acknowledgements

This research is supported by the Program of Introducing Talents of Discipline to Universities (NO. B16025). Appreciations are extended to Covestro for providing the Desmopan DP 9852 TPU pellets used in this study.

References

[1] Z. Xue, J. W. Hutchinson, Preliminary assessment of sandwich plates subject to blast loads, International Journal of Mechanical Sciences 45 (2003) 687–705.

[2] S. A. Tekalur, A. E. Bogdanovich, A. Shuklar, Shock loading response of sandwich panels with 3-D woven E-glass composite skins and stitched foam core, Composites Science and Technology 69 (2009) 736–753.

[3] K. P. Dharmasena, H. N. G. Wadley, Z. Xue, J. W. Hutchinson, Me- chanical response of metallic honeycomb sandwich panel structures to high-intensity dynamic loading, International Journal of Impact Engi- neering 35 (2008) 1063–1074.

[4] E. Wang, N. Gardner, A. Shukla, The blast resistance of sandwich com- posites with stepwise graded cores, International Journal of Solids and Structures 46 (2009) 3492–3502.

[5] M. Z. Hassan, Z. W. Guan, W. J. Cantwell, G. S. Langdon, The influence of core density on the blast resistance of foam-based sandwich structures, International Journal of Impact Engineering 50 (2012) 9–16.

[6] C. Qi, S. Yang, L. J. Yang, Z. Y. Wei, Z. H. Lu, Blast resistance and multi-objective optimization of aluminum foam-cored sandwich panels, Composite Structures 105 (2013) 45–57.

[7] Z. W. Guan, A. Aktas, P. Potluri, W. Cantwell, G. Langdon, G. Nurick, The blast resistance of stitched sandwich panels, International Journal of Impact Engineering 65 (2014) 137–145.

[8] W. Fairbairn, An Account of the Construction of the Britannia and Conway Tubular Bridges, John Weale, London, (1849).

[9] J. Zhou, M. Z. Hassan, Z. W. Guan, W. J. Cantwell, The low veloc- ity response of foam-based sandwich panels, Composites Science and Technology 72 (2012) 1781–1790.

[10] G. S. Langdon, W. J. Cantwell, Z. W. Guan, G. N. Nurick, The response of polymeric composite structures to air-blast: a state-of-the-art, Inter- national Materials Reviews 59 (2014) 159–177.

[11] M. Xu, G. Huang, S. Feng, X. Qin, G. J. McShane, W. J. Stronge, Per- foration resistance of aluminum/polyethylene sandwich structure, Ma- terials and Design 100 (2016) 92–101.

[12] J. Yi, M. C. Boyce, G. F. Lee, E. Balizer, Large deformation rate- dependent stress-strain behaviour of polyurea and polyurethanes, Poly- mer 47 (2006) 319–329.

[13] A. Jamil, Z. W. Guan, W. J. Cantwell, The static and dynamic response of CFRP tube reinforced polyurethane, Composite Structures 161 (2017) 85–92.

[14] A. Altunc, J. Kim, Al-Haik, M. R. Taha, Reliability-based design of blast-resistant composite laminates incorporating carbon nanotubes, Composite Structures 93 (2011) 2042–2048.

[15] P. D. Smith, J. G. Hetherington, Blast and Ballistic Loading of Struc- tures, University Oxford Press, 1994.

[16] Y. Han, H. Liu, Finite element simulation of medium-range blast loading using LS-DYNA, Shock and Vibration 2015 (2015) 1–9.

[17] G. H. Farrow, G. N. Nurick, G. P. Mitchell, Modelling of impulsively loaded circular plates using the ABAQUS finite element code, In: Sym- posium Finite element methods in South Africa; Stellenbosch, South Africa (1995).

[18] ABAQUS 6.14, Analysis User's Manual, Warrington, Chesire, Dassault Systems Simulia Corp.; 2014.

[19] G. N. Nurick, G. S. Langdon, Y. Chi, N. Jacob, Behaviour of sandwich panels subjected to intense air blast - Part 1: Experiments, Composite Structures 91 (2009) 433–441.

[20] Covestro LLC, http://www.tpu.covestro.com.

[21] K. S. Vecchio, F. Jiang, Improved pulse shaping to achieve constant strain rate and stress equilibrium in split hopkinson pressure bar testing, Metallurgical and Materials Transactions A 103 (2007) 1–5.

[22] G. N. Nurick, S. Mahoi, G. S. Langdon, The response of plates subjected to loading arising from the detonation of different shapes of plastic ex- plosives, International Journal of Impact Engineering 89 (2016) 102–113.

[23] N. Jacob, G. N. Nurick, G. S. Langdon, The effect of stand-off distance on the failure of fully clamped circular mild steel plates subjected to blast loads, Engineering Structures 29 (2007) 2723–2736.

[24] V. Tita, M. F. C. Junior, Numerical simulation of anisotropic polymeric foams, Latin American Journal of Solids and Structures 9 (2012) 259–279.

[25] J. F. Z. Petrovic, Polyurethane elastomers, Progress in Polymer Science 16 (1991) 695–836.

[26] S. Raman, T. Ngo, P. Mendis, A review on the use of polymeric coatings for retrofitting of structural elements against blast effects, Electronic Journal of Structural Engineering 11 (2011) 464–477.

[27] M. Y. Yahya, W. J. Cantwell, The blast behaviour of fiber reinforced thermoplastic laminates, Journal of Composite Materials 42 (2008) 2275–2297.

[28] G. R. Cowper, P. S. Symonds, Strain hardening and strain rate effect in the impact loading of cantilever beams, Brown University, Division of Applied Mathematics, Report No. 28.

[29] W. Q. Shen, N. Jones, Dynamic response and failure of fully clamped circular plates under impulsive loading, International Journal of Engi- neering 38 (1993) 2655–2665.

[30] G. R. Johnson, W. H. Cook, Fracture characteristics of three metals subjected to various strains, strain rates, temperatures and pressures, Engineering Fracture Mechanics 21 (1985) 31–48.

[31] D. R. Lesuer, Experimental investigations of material models for Ti-6Al-4V titanium and 2024-T3 aluminum and 2024-T3 aluminum. Tech- nical report, Lawrence Livermore National Laboratory, Livermore, CA (2000).

[32] N. Jones, Damage of plates due to impact, dynamic pressure and explo- sive loads, Latin American Journal of Solids and Structures 10 (2012) 767–780.

Table 1: Description of blast test specimens.

Series	Description
A	5 mm TPU core (no skins)
B	5 mm TPU core with 1.2 mm 2024-T3 skins Avg. thickness 7.75 mm
C	10 mm TPU core with 1.2 mm 2024-T3 skins Avg. thickness 12.50 mm
D	20 mm TPU core with 1.2 mm 2024-T3 skins Avg. thickness 22.60 mm

Table 2: Charge mass and diameter, impulse, failure and back face deflection for the specimens. T - full tearing and PT - partial tearing around the boundary

ID	Charge mass (g)	Charge diameter (mm)	Impulse (Ns)	Failure mode	Back face mid-point deflection (mm)
A1	8	20	11.81	I	12.17
A2	9	20	12.43	I	13.80
A3	10	20	13.09	I	14.03
A4	11	20	13.87	I	14.10
A5	12	20	14.88	II*	PT
B1	11	20	13.95	I	13.44
B2	12	20	14.68	I	13.84
B3	13	20	15.81	I	15.14
B4	14	30	18.04	II	T
C1	9	30	14.35	I	13.15
C2	10	30	17.17	I	13.57
C3	11	30	18.44	II*	PT
D1	9	30	14.13	I	5.24
D2	11	30	18.40	I	12.24
D3	13	30	23.74	I	15.33
D4	15	30	24.65	II*	PT

Table 3: Comparison of various specimens subject to uniform blast loading with comparisons made against areal density (kg/m^2), approximate material cost (GBP/kg), SOD (mm) and resistance to impulse (Ns) prior to failure.

Specimen	Areal density (kg/m^2)	Material cost (GBP/kg)	SOD (mm)	Impulse (Ns)
TPU (A4)	5.75	2.62 - 3.19	90	13.87
AA/TPU (B3)	12.32	4.22 - 4.99	90	15.81
CF/PEI [27]	12.41	26.29 - 29.24	90	14.00
GF/PEI [27]	8.60	17.12 - 24.14	90	7.93
Stitched panels[1] [7]	4.91	45.41 - 48.65	90	9.93
Mild steel [23]	14.61	0.41 - 0.42	50-100	17.94-25.36

[1] Three-dimensional woven S-glass/epoxy skins and a crosslinked PVC core

Table 4: Material properties and parameters for TPU used in the finite element modelling.

Properties	Value
Young's modulus, E (MPa)	158
Poisson's ratio, v	0.4
Density, ρ (kg/m^3)	1150
Strain-rate (s^{-1})	0.001
Fracture strain for ductile damage	2.9
Stress triaxiality	0.33

Table 5: Isotropic hardening data for TPU.

Yield stress (MPa)	11.05	25.92	45.36	119.02	265.26	295.43	390.17
Plastic strain	0	0.36	0.76	1.42	1.90	2.18	2.97

Table 6: Johnson-Cook parameters and the assumed elastic properties for AA 2024-T3 [31].

ρ (kg/m^3)	E (GPa)	v	A (MPa)	B (MPa)	n	C	m	$\dot{\bar{\varepsilon}}_0$
2740	73.09	0.33	349	426	0.73	0.0083	1	0.001

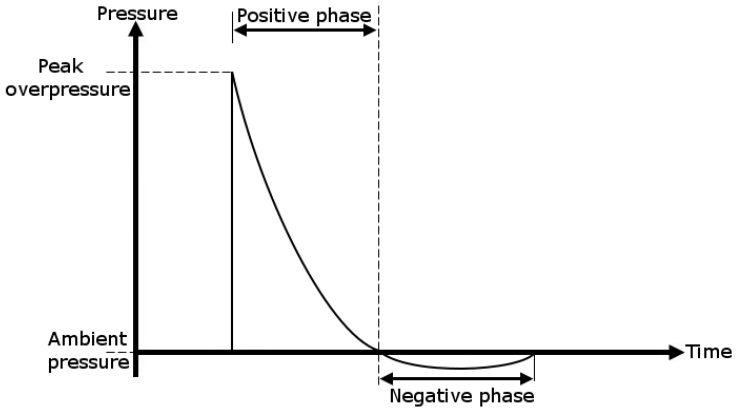

Figure 1. Typical pressure-time history from a far-field explosion.

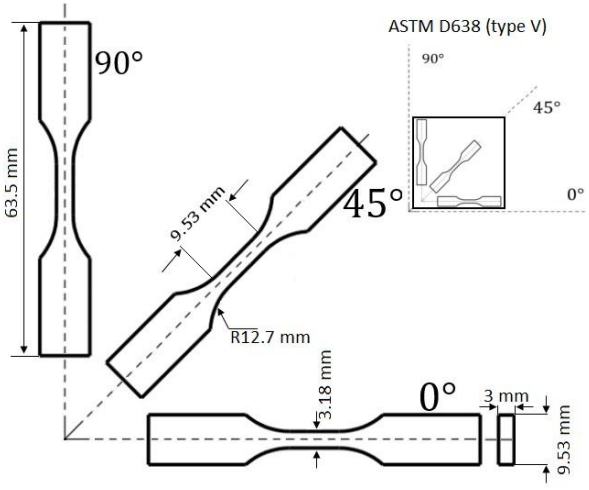

Figure 2. Geometry of the TPU tensile specimens (ASTM D638 - type V).

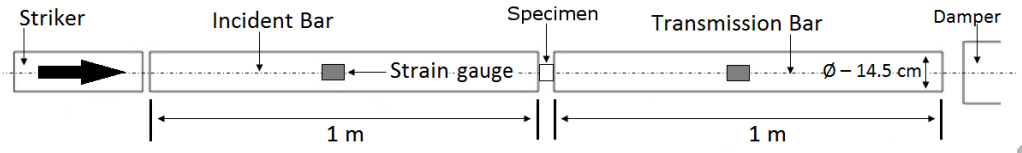

Figure 3. Schematic of the compression SHPB test set-up.

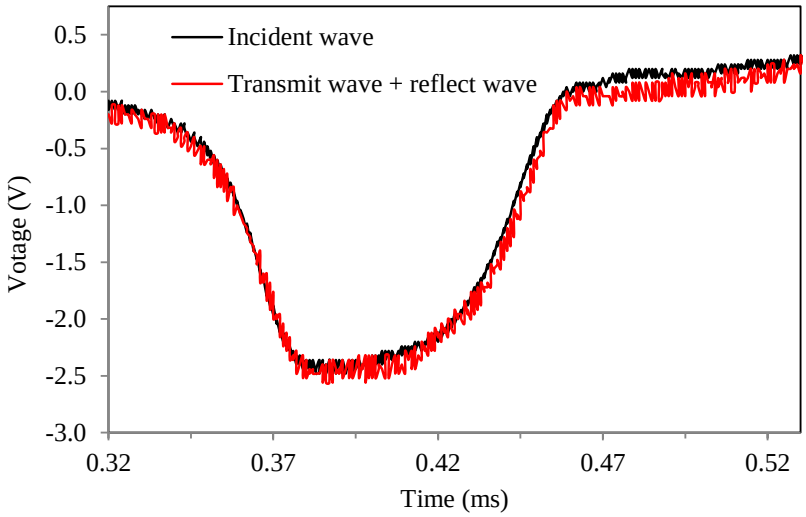

Figure 4. Proof of stress equilibrium.

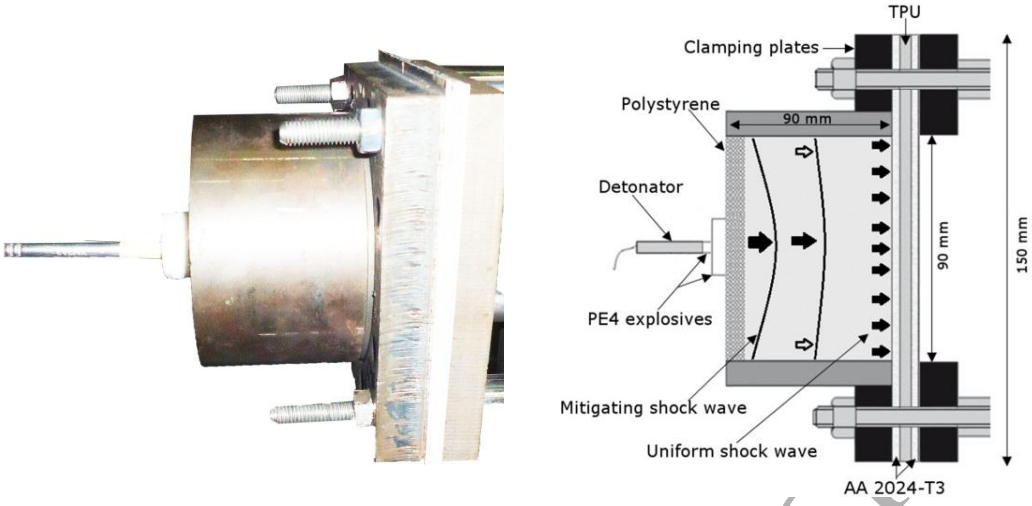

(a) Photograph (b) Schematic

Figure 5. Photograph and schematic of the air-blast test arrangement.

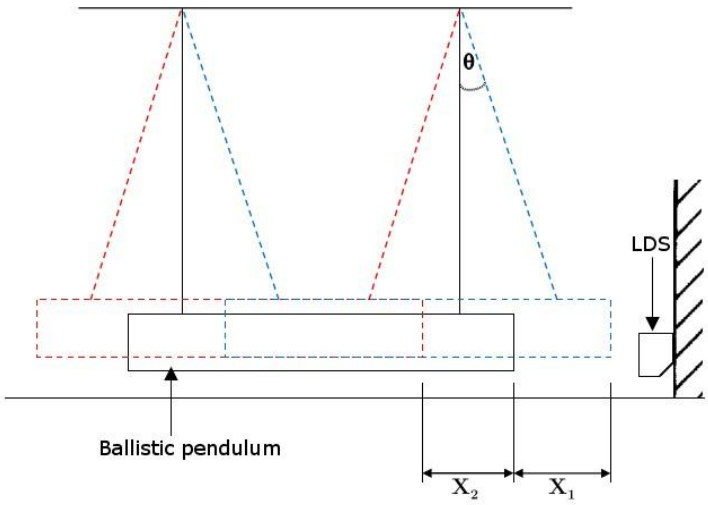

Figure 6. Schematic of the ballistic pendulum.

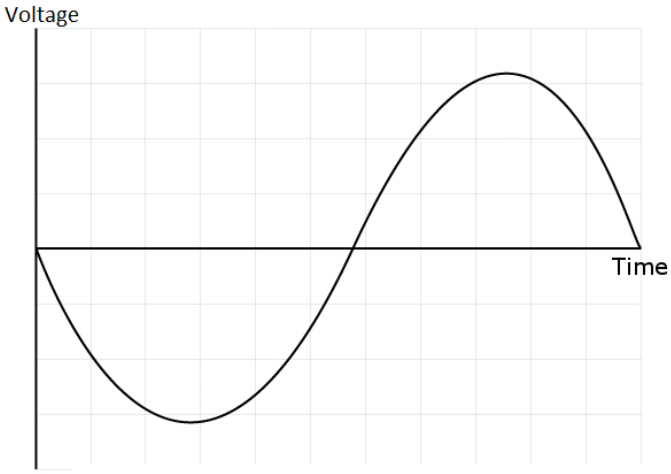

Figure 7. Sine wave output from oscilloscope.

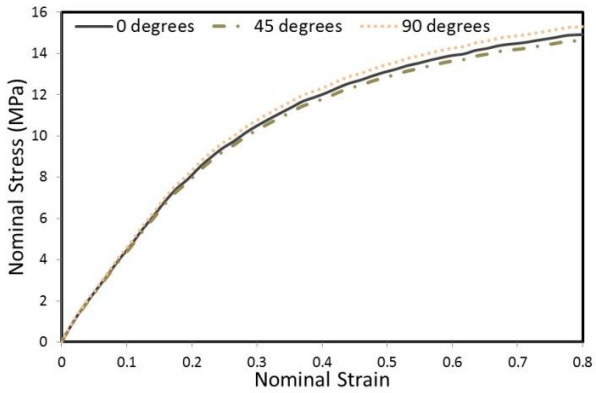

Figure 8. Stress-strain curves at three different orientations of 0°, 45° and 90°.

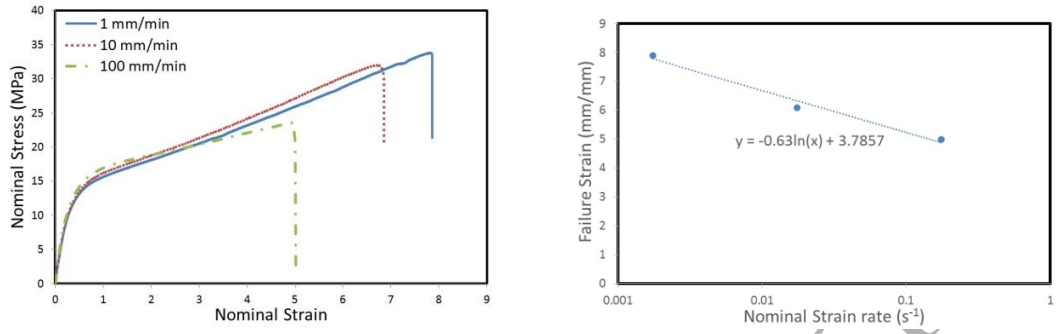

(a) Stress vs. strain. (b) Failure strain vs. strain-rate.

Figure 9. Nominal stress-strain curves (a) for TPU under tensile loading and nominal failure strains (b) for increased strain-rate loading.

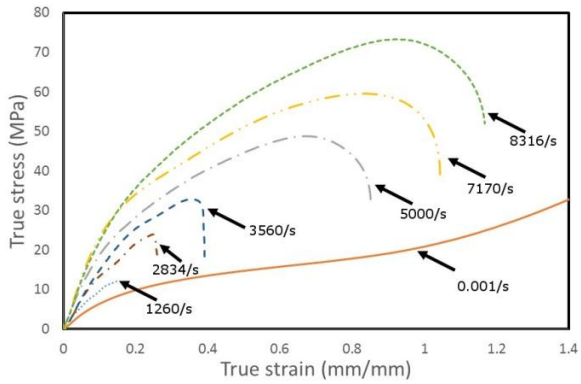

Figure 10. Compressive true stress vs. true strain for TPU at various strain-rates from SHPB tests.

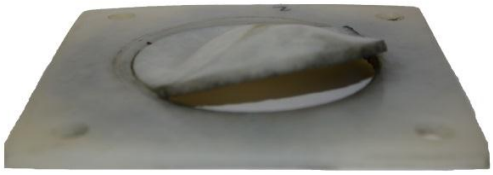

Figure 11. Partial tearing failure of TPU without skins (A5) subject to an impulse of 14.88 Ns.

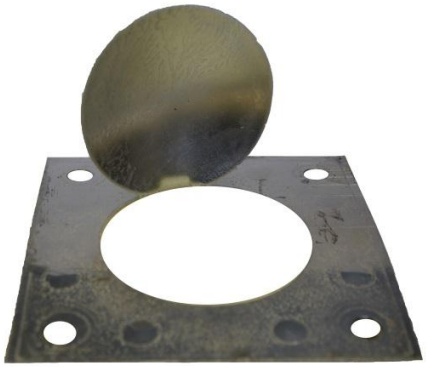

Figure 12. Back face tearing failure of an AA/TPU/AA panel (C3) subject to an impulse of 18.44 Ns.

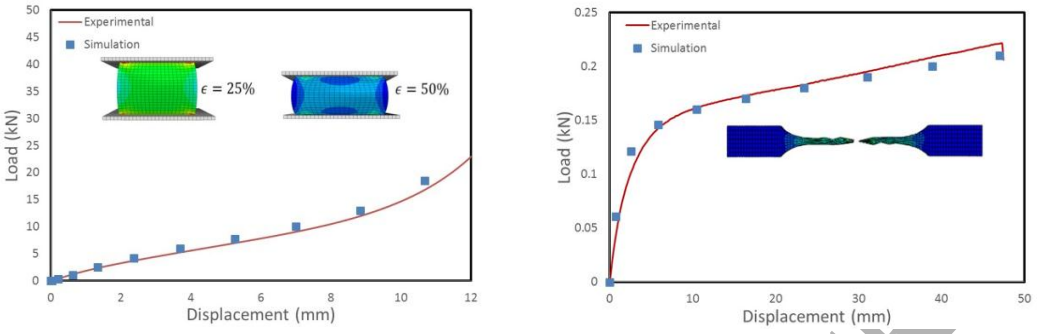

(a) Compression (b) Tension

Figure 13. Comparison of the experimental and numerical load vs. displacement response in (a) for compression and (b) tension.

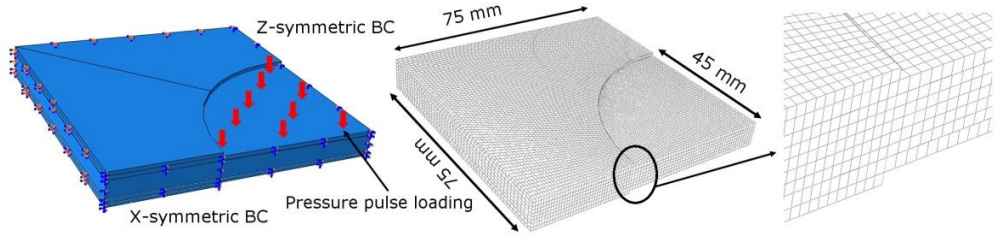

Figure 14. Dimensions, loading, boundary conditions and mesh generation of quarter model sandwich panel.

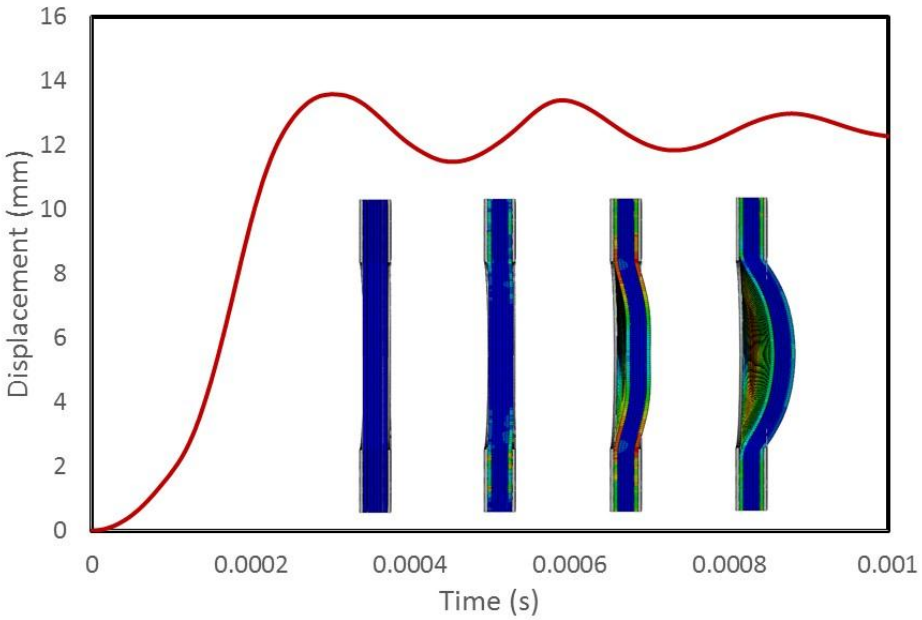

Figure 15. Typical displacement vs. time history for the blast simulations (B1).

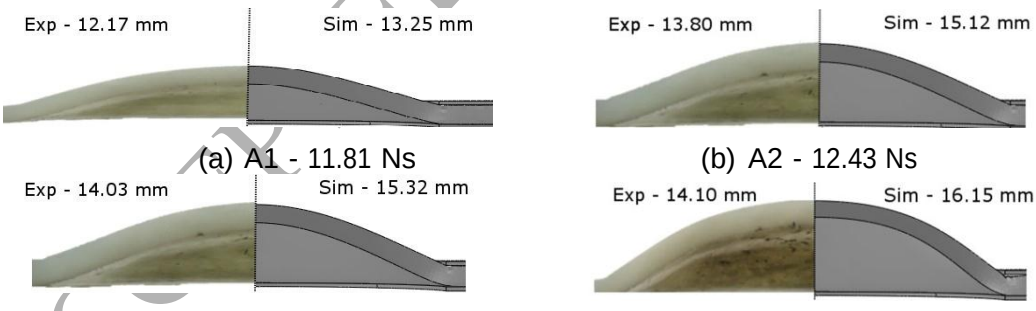

(a) A1 - 11.81 Ns (b) A2 - 12.43 Ns

(c) A3 - 13.09 Ns (d) A4 - 13.87 Ns

Figure 16. Experimental (left) vs. numerical (right) blast response.

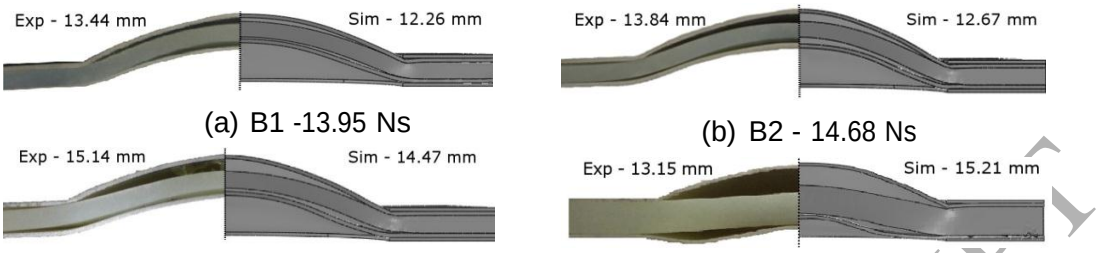

(a) B1 -13.95 Ns (b) B2 - 14.68 Ns

(c) B3 - 15.81 Ns (d) C1 - 14.35 Ns

Figure 17. Experimental (left) vs. numerical (right) blast response.

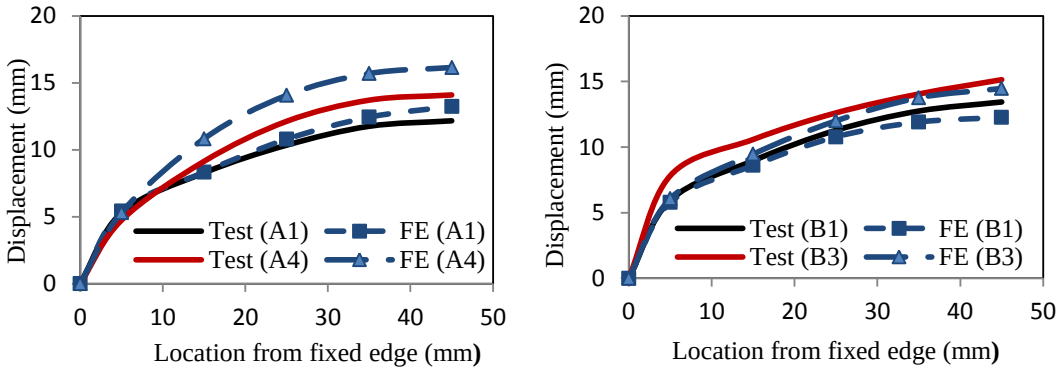

(a) panels without aluminium skins, (b) panels with aluminium skins

Figure 18. Comparisons of the measured and predicted displacement profiles at the central cross sections.

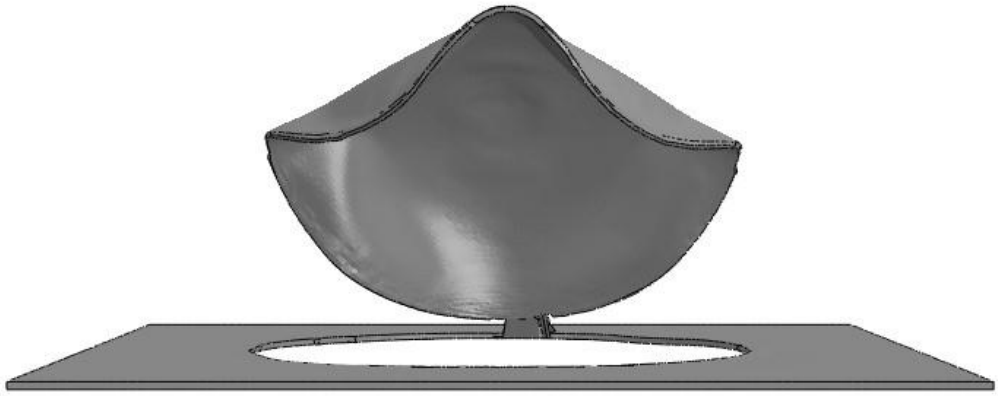

Figure 19. Numerical blast response of the back face partial tearing failure of specimen C3 (18.44 Ns).